Progress In Electromagnetics Research, PIER 104, 313–331, 2010

OPTIMIZING NANO-OPTICAL ANTENNA FOR THE ENHANCEMENT OF SPONTANEOUS EMISSION

H. Gao, K. Li, F. M. Kong, H. Xie, and J. Zhao

School of Information Science and Engineering
Shandong University
Jinan, China

Abstract—We study the characteristics of nano-optical antenna made of two gold nano-particles by three dimensional numerical calculations in visible and near infrared bands. To carry the computational burden and guarantee the precision and speed of a three dimensional FDTD calculation, adaptive mesh refinement technology is used. In this paper, we first highlight the concrete way of controlling the emitter position and orientation to fulfill the requirements of larger spontaneous emission enhancement. Then, we analyze the far field distribution and find that the far field directivity is strongly influenced by surface plasmon polaritons (SPPs). Choosing the incident wavelength of 600 nm, we compute the decay rates and radiant efficiency as a function of antenna geometry limitations. Next, the particle aspect ratio is optimized, and we obtain that $L/R = 4$ is the best for our optical-antenna. Furthermore, we present a spectrum analysis. Around 5000 fold spontaneous emission enhancement is successfully achieved. Finally, we find a piecewise linearity relationship between the particle length and resonant wavelength.

1. INTRODUCTION

Last decade has witnessed an increasing interest in electromagnetic properties of metal-dielectric structures including metallic nano-particles [1–5], nano-scale narrow metallic structures [6], and nano-scale metallic waveguide [7, 8]. In these previous researches, evident enhanced electromagnetic field and large density of states are obtained because SPPs excited at the surface of sharp tips can interact strongly

Corresponding author: F. M. Kong (kongfm@sdu.edu.cn).

with optical fields and confine far-field radiation into a localized, sub-diffraction limited volume [9]. As first proposed by Purcell [10], the decay rate can be enhanced or suppressed if one is able to modify accordingly the local density of states of the electromagnetic field in the environment where the emitter is placed. So SPPs can be used to control the radiation rate of the excitation and improve the quantum yield. In this respect, several theoretical and experimental realizations have been studied, such as emitters close to interface [11, 12], nano-spheres [13], nano-rings [14], inside cavities [15, 16], and photonic crystals [17–19].

Recently, Rogobete et al. have conducted a very helpful study of emitters close to different shapes of nano-particles and brought forward four key design principles for achieving a very strong enhancement of spontaneous emission with minimal suffering from nonradiative loss [20]. Then, a detailed exploration of limitations including the volume, size, and shape of the antenna which could yield even better performance is shown in the work of Mohammadi et al. [21]. However, considering the computational burden, the speed of calculation, and the feasibility of using body of revolution (BOR) FDTD method, their models have to be limited to emitters located and oriented such that the system preserves cylindrical symmetry.

Now, the progress in nano-optics has made possible the investigation of configurations where a single molecule is at a controlled distance from a gold nano-particle [22, 23]. To fulfill the requirements of larger spontaneous emission enhancement, we carefully studied several systems which do not satisfy the cylindrical symmetry. More exactly, the concrete influences of different emitter orientations and positions are checked. Following Mohammadi, we carefully examine two antenna models comprised of a pair of gold nano-rods (PNRs) and a pair of gold nano-ellipsoids (PNEs), respectively. And we note that, the gap distance between two nano-particles is set much smaller in these two models to achieve stronger spontaneous emission according to Rogobete's results [20]. To carry the computational burden and guarantee the precision and speed of 3D FDTD method, the adaptive mesh refinement (AMR) technology [24, 25] is used in our FDTD calculations.

In this work, we first carefully check the influence of the emitter orientation and position on spontaneous emission enhancement, and plot the near electric field distribution of our system. Then we compute the far field directivity of our optical antennas with different particle lengths, showing that the emission pattern will not stay dipolar when particle length is large enough. Choosing the incident wavelength of 600 nm, we perform a detailed analysis and comparison of the optical

properties of both antenna models as a function of their different geometrical limitations. And we successfully optimize the aspect ratio to improve the spontaneous emission of single emitter. Furthermore, a detailed spectrum analysis in the visible and near-infrared band of these antennas and an exact relationship between particle length and incident wavelength are provided in the last part of this paper.

This paper is organized as follow: Section 2 describes the models and computational approach we used; the optical characteristics of our antennas are discussed in Section 3 and a conclusion is presented in the last section.

2. ANTENNA MODELS AND COMPUTATIONAL APPROACH

The plan of our calculation models is shown in Fig. 1, where (a) and (c) stand for PNRs while (b) and (d) for PNEs. Here we note that, all through our calculation, isotropic, linear, and non-magnetic medium is considered.

In Fig. 1, each of the nano-rods is made of a cylinder with two hemispherical rounded ends, and L is the total length (the height of the cylinder plus the diameter) of one nano-particle. Whereas each nano-ellipsoid is transformed from a sphere by drawing it out in z direction and L is tip-to-tip length. For both PNRs and PNEs, G is the distance of the gap between two nano-particles, and R is the radius of the original sphere. Figs. 1(a) and (b) show the electric dipole emitter placed along with the antenna long axis while (c) and (d) show the one placed perpendicular to that. Note that, in this paper, the electronic transition of the quantum emitter is approximated as a pure electrical dipole and represented by a classical dipole (The blue short line with a red arrow showing the orientation).

In this paper, three-dimensional field distribution is calculated

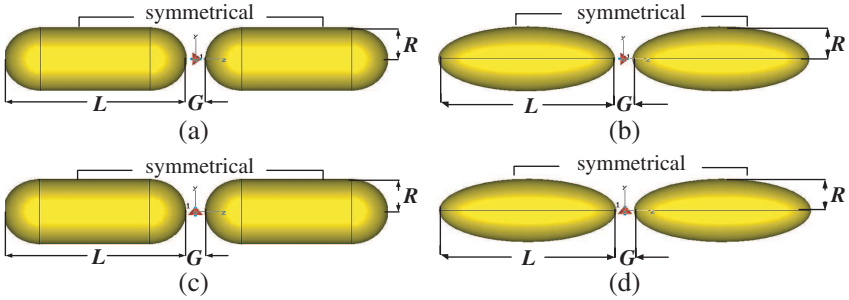

Figure 1. The antenna models designed in FDTD calculation.

using the FDTD method [26], which is simply a space and time discretization of the Maxwell curl equations [27]. Before introducing the calculation approach of decay rates, the dispersion model of metal at optical wavelengths is discussed at first. Because the perfect conductor approximation is not valid when the metallic nanostructures are studied at visible and near-infrared band, the dispersive negative dielectric function of the metals must be taken into account. And as negative values of ε cannot be directly included in the standard set of Maxwell's equations, special techniques are necessary to allow the FDTD calculation to proceed. In our calculation, to simulate gold nano-particles, a modified Drude dielectric function is employed:

$$\varepsilon(\omega) = \varepsilon_\infty - \frac{\omega_p^2}{\omega^2 + j\omega\gamma} \tag{1}$$

where ε_∞, ω_p and γ stand for the dielectric constant for the frequency going to the infinite, the plasma frequency, and the relaxation frequency of the metal, respectively.

The modified Drude dielectric model is fitted to a particular frequency range of Johnson and Christy bulk dielectric data [28]. For gold, the parameters we used are $\varepsilon_\infty = 9.5$, $\omega_p = 8.9488\,\text{eV}$ and $\gamma = 0.06909\,\text{eV}$. A comparison of our fitted Drude model to the bulk values for gold is shown in Fig. 2. The square dots are the real part and the round ones are the imaginary part of the Johnson and Christy bulk dielectric data for gold. While the solid line shows the real part and dashed line shows the imaginary part of our modified Drude fit. Obviously, in the region of 500–900 nm, our model agrees to the experimental data well.

Although BOR technique in the FDTD method can reduce the original three dimensional problem to a two dimensional one, we still cannot use this method in our calculation because our several models do not satisfy the requirements of cylindrical symmetry. As the modeling of the nanostructures requires fine meshes to resolve the geometrical features, mesh size Δs has to be set small enough to insure the accuracy. Moreover, our calculation needs the distribution of the far field to get the Purcell factor, antenna efficiency, and angular directivity. This means the integral region's radius must be more than one wavelength. So the simulation domain must be large enough. In our paper, calculation regions are $2000\,\text{nm} * 2000\,\text{nm} * 2000\,\text{nm}$ for both PNRs and PNEs. However, the FDTD mesh has to be limited to a finite region of space to store the field variables and the auxiliary quantities in the computer memory. In other words, to save memory and CPU time, it is convenient to reduce the simulation domain as much as possible. An efficient technology that fulfills the entire requirement mentioned above is the so-called adaptive mesh

refinement (AMR) [24, 25], which we have chosen for our FDTD calculation. More exactly, in our approach, the first step is creating initial mesh. And the minimum grid size plus the maximum one are both set first here, which are 1 nm and 20 nm, respectively. While the electromagnetic field simulation is performed, the energy density in the computation domain is recorded. Regions with high energy density and high field gradients are identified, and the mesh is locally refined there. To mitigate the numerical errors, the Delta S quantity is defined as the maximum deviation of the S-parameters between two subsequent passes. Note that, this deviation is calculated by determining the actual distance between the corresponding curves in the complex plane rather than simply doing a frequency-by-frequency comparison. Small shifts in resonance frequencies therefore cause small differences only. Furthermore a weighting function is applied decreasing the contribution of errors at frequencies further away from the center of the frequency band. The mesh adaptation would not stop until the S-parameters converge such that the Delta S value falls below a certain limit (2% in our calculation). Moreover, perfectly matched layer surrounds the entire simulation domain [29, 30] (PML) to absorb outgoing waves and avoid non-physical reflections in our calculations.

As Ruppin and Agio et al. [13, 31] have shown that, improving florescence of a single emitter with a nano-optical antenna requires systems that deliver a strong local electric field E, a large Purcell factor F, and high antenna efficiency η_a which is near 100% at the same time. And Xu et al. [16] have also pointed out that the ratio of the decay rate can be substituted by the ratio of the power. Then,

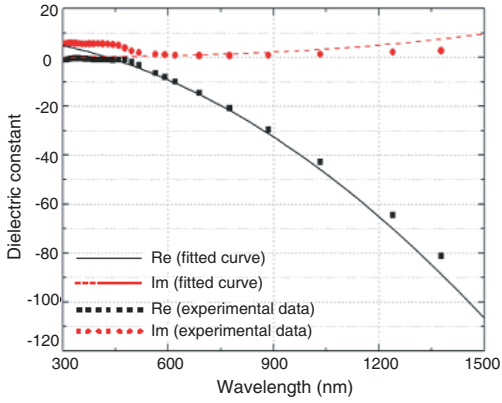

Figure 2. Comparison between the Johnson and Christy bulk dielectric data for gold and our modified Drude fit.

to determine the emission rates and directivity for various emitter antenna configurations, a general approach is only to calculate the electromagnetic field and the power distribution produced by a single emitter in proximity to a metallic nano-particle. Note that, the electronic transition of the quantum emitter is approximated as a pure electrical dipole emitter here and represented by a classical point dipole. Besides, an electric dipole emitter in vacuum ($\varepsilon = 1$) is used as a reference for the calculation.

Following Taminiau [32], the radiative decay rate enhancement (Purcell factor) F is taken in our calculation as:

$$F = \frac{\iint P(\varphi, \theta) d\Omega}{\iint P_0(\varphi, \theta) d\Omega} \tag{2}$$

where $P(\varphi, \theta)$ and $P_0(\varphi, \theta)$ are the power radiating to the far field for the system understudy and for the reference dipole in vacuum, respectively. And the non-radiative decay rate K_{nr} is taken as:

$$K_{nr} = \frac{R_{diss}(r, \theta, \varphi)}{\iint P_0(\varphi, \theta) d\Omega} \tag{3}$$

where $R_{diss}(r, \theta, \varphi)$ is the total power dissipated in the metal. We noted that, the angles φ and θ are the usual azimuthal and polar angles in spherical coordinates. And the integration is performed over the full spherical surface with the radius which is far larger than one wavelength. Then the total efficiency for emission into the far field (commonly called antenna efficiency) η_a can be written as

$$\eta_a = \frac{\iint P(\varphi, \theta) d\Omega}{\iint P(\varphi, \theta) d\Omega + \iiint R_{diss}(r, \theta, \varphi) dV_{metal}} \tag{4}$$

Finally, in the far field calculation, to characterize the angular dependence of the emitted intensity, the angular directivity $D(\varphi, \theta)$ is defined as [32]:

$$D(\varphi, \theta) = \frac{4\pi P(\varphi, \theta)}{\iint P(\varphi, \theta) d\Omega} \tag{5}$$

3. RESULTS AND DISCUSSION

In this section, the influence of the electric dipole orientation and position will be compared first, followed by the far field directivity analysis. Then the optimization of antenna shape factor to obtain large Purcell factor and high antenna efficiency for both PNRs and PNEs will be discussed in details. Finally, the spectrum analysis where incident wavelength varies from 500 nm to 900 nm will be explored.

3.1. Influence of the Electric Dipole Orientation and Position

As we know, the electric dipole placed in the middle of the gap between two nano-particles has two different orientations. The one is perpendicular to the antenna long axis and the other is parallel to that. Fig. 3 shows the view of the different power flow distributions in $y = 0$ plane, where (a) and (c) are the results of PNRs and the other two belong to PNEs. The electric dipole is perpendicular to the long antenna axis in (a) and (b), while it is changed to be parallel to that axis in (c) and (d). From this figure, both PNRs and PNEs highly confine the power in local field when the emitter orientation is perpendicular to long antenna axis, especially for PNEs. But that power is allowed to radiate to the far field as long as the emitter orientation is parallel to the antenna axis.

This could be explained as follows. The nano-particles are in the place where the zenith angle $\theta = 90^\circ$ for (a) and (b). According to classical electrodynamics' theory, the magnetic field H_φ must be taken

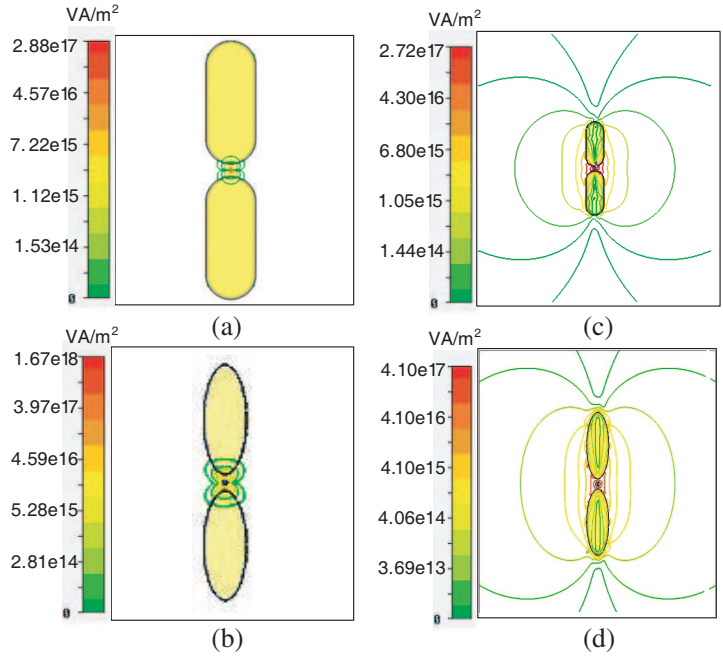

Figure 3. Top view (in xoy plane) of the power flow distribution. Both the two models have the same geometrical parameters ($L = 100\,\text{nm}$, $R = 20\,\text{nm}$, and $G = 10\,\text{nm}$).

into account. But when we calculate the average Poynting power, we find that:

$$\vec{S}_{rav} = \frac{1}{2}\mathrm{Re}(\vec{E} \times \vec{H}^*) = 0 \tag{6}$$

That means the energy is transforming between the electric form and the magnetic one. So, the field near the antenna is an inductive field, which will not radiate power far. But in the condition of (c) and (d), the zenith angle is changed to be zero. All the magnetic field components are equal to zero. That means the effect of the magnetic field on the metallic nano-particles can be ignored. Our gold nano-particles are only influenced by the electric field, which makes positive charges gather in one tip of the nano-particles while free electrons assemble at the other end at the same time. Therefore, these particles can be seen approximately as some newly formed electric dipole emitters with the same orientation as the original one. And they can be very helpful to the enhancement of the spontaneous emission.

In the work of Mohammadi [21], displacement of the emitter along the nano-particle axis away from the center was performed. They pointed out this displacement can modified the emission pattern and get stronger enhancement. However, those models are limited to emitters located such that the system preserves cylindrical symmetry. To further discuss the influence of emitter position, we displace the emitter 2 nm away from the nano-particle axis (see the inset of Fig. 4) and compare its Purcell factor and antenna efficiency with those of emitter placed in the center of nano-antenna gap. All these results are shown in Fig. 4, where (a) for PNRs and (b) for PNEs. And we note that, the particle length, radius and gap distance are 80 nm, 20 nm, and 20 nm, respectively.

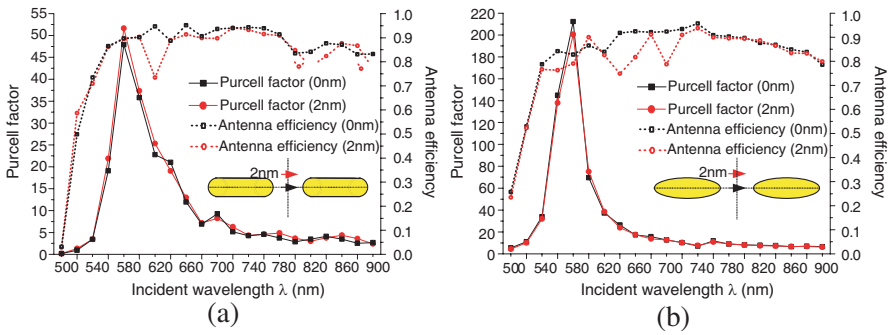

Figure 4. Antenna efficiency η_a (dashed curves) and Purcell Factor F (solid curves) for an emitter coupled to two gold nano-particles separated by 20 nm for various emitter positions.

Comparing Fig. 4(a) and Fig. 4(b), we can easily find that the PNEs have larger Purcell factors than PNRs at the same wavelength. These results fully accord with the former conclusion drawn by Rogobete [20] and Mohammadi [21]. Moreover, we note that, in Fig. 4(a), the Purcell factor F is larger when we display the emitter 2 nm away from the nano-particle axis. While in Fig. 4(b), that Purcell factor F is smaller. However, there is not much difference for both PNRs and PNEs. As to the antenna efficiency, both (a) and (b) show that η_a has a decrease if we display the emitter 2 nm away from the nano-particle axis. And this indicates that displacing the emitter will make more power be lost in the metallic nano-particles.

In a word, although the displacement of emitter will get larger Purcell factor for PNRs, there is no marked difference in the spectrum from 500 nm to 900 nm. Besides, that displacement will cause greater loss and lower antenna efficiencies. Then, in order to get high Purcell factor and make more efficient optical antennas, we will only discuss those systems with the emitter oriented along the nano-particle axis and just placed in that axis.

3.2. Far Field Directivity Analysis

Considering the current distribution mentioned above, when the original emitter is parallel to the particle long axis, our models can be seen as dipoles, which are one of the simplest but most widely used antenna. However, because of the excited SPPs, far field distribution of our optical antennas will be strongly influenced. To further explore this effect, we then calculate the angular directivity of the entire system while turning the particle length. All results are plotted in Fig. 5. Where (a) is an overview of the system considered and (b) is the angular directivity of the electric dipole placed in the vacuum as a reference. All nano-particles have same radius of 20 nm and the gap distance of 10 nm. The incident wavelength we used is 600 nm.

Figures 5(c) and (d) show the corresponding angular directivity for the emitter coupled to PNRs and PNEs with different length. Obviously, dipolar emission patterns are obtained in most cases, with a maximum directivity ranging from 1.5 to 2.0. As the length of the particle increases to 140 nm, the maximum directivity augments while the angular width minishes for both PNRs and PNEs. And the main lobe direction is all the same as the pattern of emitter itself. This results highly accord with the former work of Rogobete et al. [20]. But it is interesting to note that, the dipolar emission patterns are not so obviously as the former ones and the side lobe is generated when the length of the particle reaches 180 nm. Especially for PNEs, the 'side lobe' is so remarkable that it replaces the original main lobe,

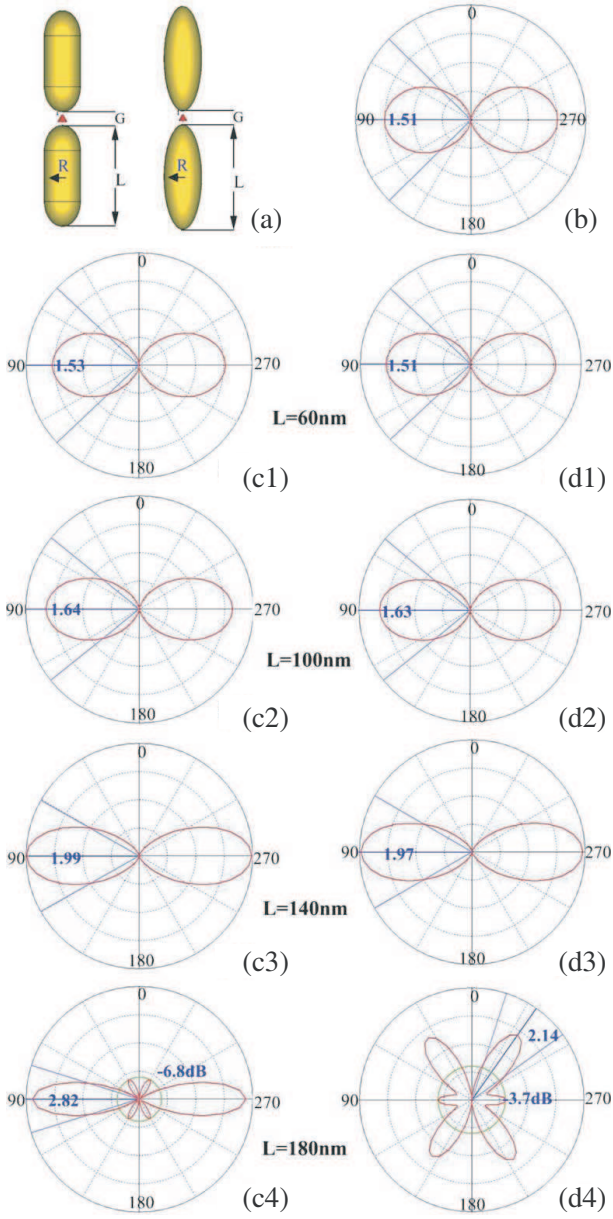

Figure 5. Angular directivities for the configurations of PNRs and PNEs with different particle length L.

and changes the main direction by 55 degrees. The dipolar radiation pattern is lost!

Obviously, the source of this system's angular emission is a combination of the dipole moment of emitter, plus the response of antenna, and the moment of antenna mode [32]. We also note that, for dipole antennas, they have non-dipolar emission because of their higher modes when the total length $2l$ is larger than one incident wavelength λ [33]. But in our results, side lobe occurs for both PNRs and PNEs when the particle length L reaches 180 nm. In other words, the total length $2l$ is only 370 nm, which is much small than one wavelength. That is because SPPs exist in the tip of our gold nano-particles, which make higher modes be excited more easily and influence the far field directivity. Comparing our results shown in Figs. 5(c) and (d), we can easily find that, larger side lobe occurs for PNEs. And this also proves that far field directivity can be influenced by SPPs, since SPPs in PNEs are stronger than those in PNRs.

3.3. Optimization of the Geometrical Parameters

Several theoretical and experimental realizations [13, 20, 21, 32] have shown that different geometric parameters will change the performance of original electric emitter. In this section, we optimize the geometrical limitations of our nano-optical antenna and want to get larger Purcell factor and higher antenna efficiency. Considering the wavelength of red light which we usually select is around 600 nm, we choose 600 nm as our incident wavelength in the following simulations.

First, we note that the Purcell factors for both of the two kinds antennas decrease as the gap-distance becomes larger [20]. This is because the magnitude of the electric field caused by the dipole emitter is proportional to $1/R^3$. The coupling of the emitter to the antenna mode will be very weak when the gap is wide enough. Very little power is lost in the metallic nano-particles while most of that is radiated to the far field in the same way as the electric dipole emitter placed in the vacuum. So, in order to get large spontaneous emission enhancement, we must make the gap of two particles be small enough, as long as the manufacture technique permits. However, because of the convenience and accuracy of our simulation, the gap distance is fixed to be 10 nm and no smaller distance is chosen in our following research.

We vary the shape factor of each particle by first turning the particle length and then widening the particle radius to further explore the influence of geometrical parameter on emission enhancement and antenna performance. All these results are shown in Fig. 6 and Fig. 7. Fig. 6 is the results when particle radius fixed to be 20 nm while Fig. 7 shows the results of particle length fixed to be 100 nm.

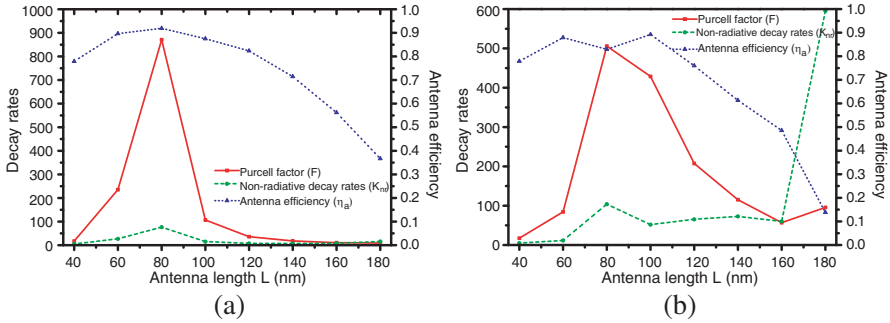

Figure 6. Antenna efficiency and decay rates spectrum for different shape factors of the nano-particles with $G = 10$ nm, where (a) shows the results of PNRs while (b) stands for PNEs. Each particle has fixed radius of 20 nm and its length is varied from 40 nm to 180 nm with the step of 20 nm.

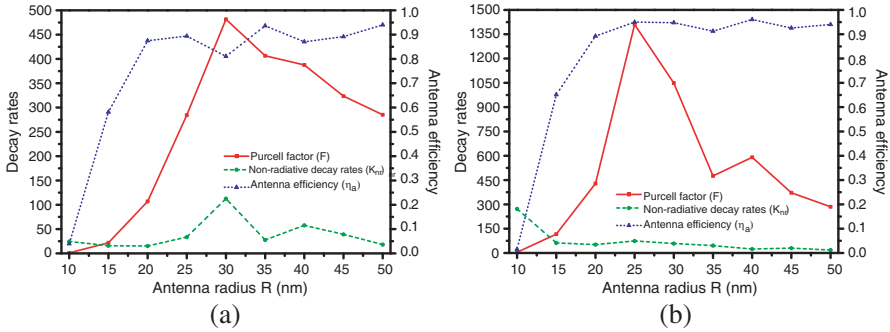

Figure 7. Antenna efficiency and decay rates spectrum for different shape factors of the nano-particles with $G = 10$ nm, where (a) shows the results of PNRs while (b) stands for PNEs. Each particle has fixed length of 100 nm and its radius is widened from 10 nm to 50 nm with the step of 5 nm.

Before evolving our discussion, we first parameterize the shape factor of one particle by the L/R ratio, where L is the length of one particle and R is the radius of that. Then we compare Fig. 6(a) and Fig. 6(b) and find that PNRs has stronger enhancement than PNEs at resonance. That is because the volume of PNRs is larger than that of PNEs when they have same shape factor. Then larger localized field enhancement can be excited. However, as shown in Fig. 6 and Fig. 7, for most settings, PNEs have larger emission enhancement than PNRs with same shape factors. These results fully accord with Rogobete's

conclusion that elongated objects should be chosen to benefit from strong near field at sharp corners [20]. And according to the conclusion in Mohammad's work [21], increasing the shape factor can cause steep decrease of the Purcell factor if the head of the nano-particle is flat. The localized field enhancement is rapidly lost when that kind of particle gets thicker. But we note that, in our calculation, as the length or the radius increases, the radiative decay rates rise to its peak value and then decrease rapidly. Similar trends can be seen for both PNRs and PNEs. Moreover, it should be emphasized that the peak value of the Purcell factor mostly occurs when the shape factor meets the condition of $L/R = 4$.

What's more, high Purcell factor usually comes with high non-radiative decay rate. But the radiative decay rate is the leading part at resonant which makes the antenna efficiency also stand at high level. Comparing these four figures, we can draw the conclusion that, our optical antenna gets a low efficiency when the shape factor is large enough, especially for PNEs. For example, more than 95% of power is lost in the metallic nano-particles when the PNEs is very thin, where shape factor is $L/R = 10 : 1$. That is because nano-optical antenna with very large shape factor has little plasmon resonance of the antenna lying in this spectral region [20]. Plenty of power is dispersed in the metallic nano-particles and cause huge non-radiative decay rate, leading to very low antenna efficiencies.

In conclusion, the antenna geometry should be tailored such that the plasmon resonance of the antenna lies in this favorable spectral region for minimizing the dissipation in the metal and the gap distance should be set smaller as long as the manufacture technique permits. Finally, the shape factor of nano-particle is optimized to $L/R = 4$ for achieving high emission enhancement and perfect antenna performance at 600 nm.

3.4. Spectrum Analysis

In the former section, we optimized the aspect ratio to enhance the spontaneous emission. But there's a prerequisite that incident wavelength is 600 nm. Different incident wavelength requires different aspect ratio. In order to obtain an exact relationship between the antenna structure and incident wavelength, we provide a detailed spectrum analysis as follows. The models we used in our research have same radius $R = 20$ nm and gap distance $G = 10$ nm. The electric dipole is at a fixed orientation and in the middle of the gap. Antenna lengths (L) for both PNRs and PNEs are increased from 60 nm to 160 nm with the step of 20 nm. And in the region from 500 nm to 900 nm, one monitor is set every other 10 nm.

We first consider a dipole coupled to PNRs, these results are plotted in Fig. 8. From Fig. 8(a), the emission enhancement drops rapidly to values below 500 at the incident wavelength falling out of the visible region ($\lambda > 780\,\text{nm}$) when particle length is smaller than 100 nm. When PNRs has a larger volume ($L \geq 120\,\text{nm}$), stronger decay rates enhancement can be caused in the same region. And the Purcell factor can reach the value up to 5000 at its resonance wavelength $\lambda = 880\,\text{nm}$ when $L = 160\,\text{nm}$. Another important variable is the antenna efficiency η_a. As shown in Fig. 8(b), three important aspects can be noticed. First, η_a increases as λ becomes larger. Secondly, the antenna efficiency reaches its plateau (around 90%) already at wavelength close to 550 nm when $L = 60\,\text{nm}$. And as the long axis L becomes larger, the wavelength increases from 550 nm for $L = 60\,\text{nm}$ to 700 nm for $L = 160\,\text{nm}$. Thirdly, the longer the particle length L is, the higher plateau η_a reaches.

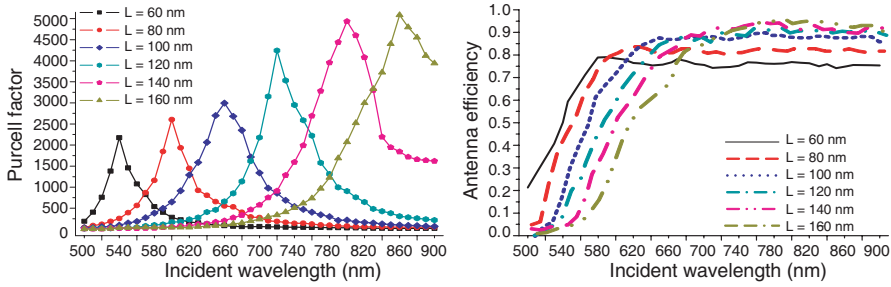

Figure 8. Purcell factors and antenna efficiencies of electric emitter coupled to PNRs for various particle length L.

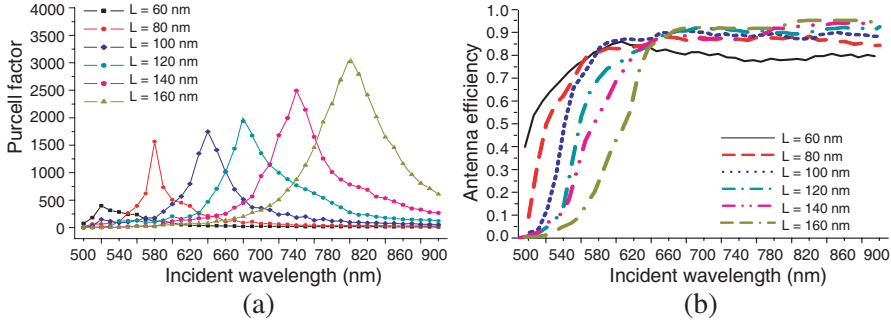

Figure 9. Purcell factors and antenna efficiencies of electric emitter coupled to PNEs for various particle lengths.

Next, we consider PNEs which have similar shape factor as PNRs but sharper ends. These results are presented in Fig. 9. Comparing to PNRs' results which are shown in Fig. 8(a), similar trends can be seen while the enhancements are much smaller at short wavelengths. Fig. 9(b) shows the antenna efficiency results of PNEs. Comparing to PNRs' results shown in Fig. 8(b), two better performances can be easily found. Antenna efficiencies reach higher level and increase more rapidly than the former in shorter wavelength.

Basing on the former analysis, the resonance wavelength of both PNRs and PNEs with various long antenna axes L is plotted in Fig. 10. Black line stands for PNRs while red one stands for PNEs. Obviously, as the long antenna axis L gets larger, the resonance wavelength λ_R shows a red shift to the near-infrared region. Comparing these results of both PNRs and PNEs, we can find that, the resonance wavelength of PNRs is larger than that of PNEs with the same long axis. For both two types antenna with large aspect ratio, the red shift of PNRs (a margin of 160 nm) is more evident than that of PNEs (a margin of 120 nm). And there is a piecewise linearity relationship between the long antenna axis L and the resonant wavelength λ_R for both PNRs and PNEs.

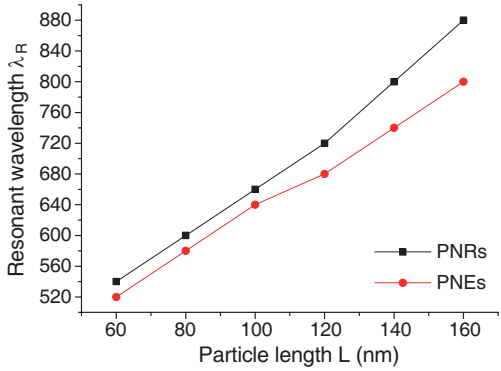

Figure 10. Resonant wavelengths as a function of particle lengths.

4. CONCLUSION

We perform a systematic analysis of two optical antenna models composed of a pair of nano-rods (PNRs) as well as a pair of nano-ellipsoids (PNEs) in this paper. Using the 3D-FDTD method, we have calculated the decay rates and antenna efficiency of an electric dipole emitter coupled to these optical antennas. In this paper, several models

do not preserve cylindrical symmetry and cannot be calculated using BOR method. But automatic mesh refinement (AMR) technology allows our study with the computational burden and speed of a 3D FDTD calculation. In our discussion, we first find the right orientation and position of the electric emitter which can radiate the local energy to the far field, cause huge emission enhancement, and have high antenna efficiency. We then perform the far field analysis of both PNRs and PNEs. From those results, we find that the dipolar emission pattern is lost as the particle length reaches 180 nm, and we successfully demonstrate that SPPs excited in the tips of our nano-particles can influence the far field directivity. Choosing the incident wavelength of 600 nm, we carefully examine the influence of shape factor on emission enhancement. Our results show that both PNRs and PNEs will get the largest emission enhancement if their shape factors meet $L/R = 4$. Finally, we perform the spectrum analysis for both antennas and obtain a piecewise linearity between the long antenna axis and the resonant wavelength.

Our results highlight the way of controlling the emitter position and the geometry parameters of the nano-particles to fulfill the experiments requirements, especially when large enhancements are desired. Mastering these properties in the laboratory will make gold nano-particles very attractive for applications in field-enhanced spectroscopy, optoelectronics and active met materials in visible and near-infrared bands.

ACKNOWLEDGMENT

This work was financed by the National Foundation of China under Contract No. 60877018, the National Basic Research Program of China (973 Program) through Grant No. 2009CB930503, 2009CB930501 and 2007CB613203.

REFERENCES

1. Mühlschlegel, P., H.-J. Eisler, O. J. F. Martin, B. Hecht, and D. W. Pohl, "Resonant optical antennas," *Science*, Vol. 308, 1607–1609, 2005.
2. Krenn, J. R., A. Dereux, J. C. Weeber, E. Bourillot, Y. Lacroute, and J. P. Goudnnet, "Squeezing the optical near-field zone by plasmon coupling of metallic nanoparticles," *Phys. Rev. Lett.*, Vol. 82, No. 12, 2590–2593, 1999.
3. Aizpurua, J., P. Hanarp, D. S. Sutherland, M. Käll, G. W. Bryant,

and F. J. García de Abajo, "Optical properties of gold nanorings," *Phys. Rev. Lett.*, Vol. 90, No. 5, 057401, 2003.

4. Nehl, C. L., H. Liao, and J. H. Hafner, "Optical properties of star-shaped gold nanoparticles," *Nano. Lett.*, Vol. 6, 683–688, 2006.
5. Fischer, H. and O. J. F. Martin, "Engineering the optical response of plasmonic nanoantennas," *Opt. Express*, Vol. 16, No. 12, 9144–9154, 2008.
6. Kong, F., K. Li, B.-I. Wu, H. Huang, H. Chen, and J. A. Kong, "Propagation properties of the SPP modes in nanoscale narrow metallic gap, channel, and hole geometries," *Progress In Electromagnetics Research*, PIER 76, 449–466, 2007.
7. Kong, F., K. Li, H. Huang, B.-I. Wu, and J. A. Kong, "Analysis of the surface magnetoplasmon modes in the semiconductor slit waveguide at terahertz frequencies," *Progress In Electromagnetics Research*, PIER 82, 257–270, 2008.
8. Kong, F., B.-I. Wu, H. Chen, and J. A. Kong, "Surface plasmon mode analysis of nanoscale metallic rectangular waveguide," *Opt. Express*, Vol. 15, No. 19, 12331–12337, 2007.
9. Ozbay, E., "Plasmonics: Merging photonics and electronics at nanoscale dimensions," *Science*, Vol. 311, No. 5758, 189–193, 2006.
10. Purcell, E. M., "Spontaneous emission probabilities at radio frequencies," *Phys. Rev.*, Vol. 69, 681, 1946.
11. Drexhage, K. H., "Interaction of light with monomolecular dye layers," *Prog. Opt.*, Vol. 12, 164, 1974.
12. Chance, R. R., A. Prock, and R. Silbey, "Molecularfluorescence and energy transfer near interfaces," *Adv. Ch. Phys.*, Vol. 37, 1, 1978.
13. Ruppin, R., "Decay of an excited molecule near a small metal sphere," *J. Chem. Phys.*, Vol. 76, 1681–1684, 1982.
14. Blanco, L. A. and F. J. Garcia de Abajo, "Spontaneous light emission in complex nanostructures," *Phys. Rev. B*, Vol. 69, No. 20, 205414, 2004.
15. Hulet, R. G., E. S. Hilfer, and D. Kleppner, "Inhibited spontaneous emission by a rydberg atom," *Phys. Rev. Lett.*, Vol. 55, No. 20, 2137, 1985.
16. Xu, Y., J. S. Vučković, R. K. Lee, O. J. Painter, A. Scherer, and A. Yariv, "Finite-difference time-domain calculation of spontaneous emission lifetime in a microcavity," *J. Opt. Soc. Am. B*, Vol. 16, 465, 1999.
17. Yablonovitch, E., "Inhibited spontaneous emission in solid-state physics and electronics," *Phys. Rev. Lett.*, Vol. 58, No. 20, 2059,

1987.

18. Hermann, C. and O. Hess, "Modified spontaneous-emission rate in an inverted-opal structure with complete photonic bandgap," *J. Opt. Soc. Am. B*, Vol. 19, 3013–3018, 2002.
19. Femius Koenderink, A., L. Bechger, H. P. Schriemer, A. Lagendijk, and W. L. Vos, "Broadband fivefold reduction of vacuum fluctuations probed by dyes in photonic crystals," *Phys. Rev. Lett.*, Vol. 88, No. 14, 143903, 2002.
20. Rogobete, L., F. Kaminski, M. Agio, and V. Sandoghdar, "Design of plasmonic nanoantennae for enhancing spontaneous emission," *Opt. Lett.*, Vol. 32, No. 12, 1623–1625, 2007.
21. Mohammadi, A., V. Sandoghdar, and M. Agio, "Gold nanorods and nanospheroids for enhancing spontaneous emission," *New J. Phys.*, Vol. 10, 105015, 2008.
22. Kühn, S., U. Hakanson, L. Rogobete, and V. Sandoghdar, "Enhancement of single-molecule fluorescence using a gold nanoparticle as an optical nanoantenna," *Phys. Rev. Lett.*, Vol. 97, No. 1, 017402-4, 2006.
23. Anger, P., P. Bharadwaj, and L. Novotny, "Enhancement and quenching of single-molecule fluorescence," *Phys. Rev. Lett.*, Vol. 96, No. 11, 113002-4, 2006.
24. Liu, Y. X. and C. D. Sarris, "AMR-FDTD: A dynamically adaptive mesh refinement scheme for the finite-difference time-domain technique," *IEEE Antennas and Propagation Society International Symposium*, Vol. 1A, 134–137, 2005.
25. Berger, M. J. and J. R. Oliger, "Adaptive mesh refinement for hyperbolic partical differential equation," *J. Comput. Phys.*, Vol. 53, 484–512, 1984.
26. Yee, K., "Numerical solution of initial boundary value problems involving Maxwell's equations in isotropic media," *IEEE Trans. Antennas Propag.*, Vol. 14, No. 3, 302–307, 1966.
27. Taflove, A. and S. C. Hagness, *Computational Electrodynamics: The Finite-difference Time-domain Method*, Artech House, Boston, 2000.
28. Johnson, P. B. and R. W. Christy, "Optical constants of the noble metals," *Phys. Rev. B*, Vol. 6, No. 12, 4370–4379, 1972.
29. Berenger, J. P., "A perfectly matched layer for the absorption of electromagnetic waves," *J. Comput. Phys.*, Vol. 114, 185–200, 1994.
30. Berenger, J. P., "Three-dimensional perfectly matched layer for the absorption of electromagnetic waves," *J. Comput. Phys.*,

Vol. 127, 363–379, 1996.

31. Agio, M., G. Mori, F. Kaminski, L. Rogobete, S. Kühn, V. Callegari, P. M. Nellen, F. Robin, Y. Ekinci, U. Sennhauser, H. Jäckel, H. H. Solak, and V. Sandoghdar, "Engineering gold nanostructures to enhance the emission of quantum emitters," *Proc. SPIE*, Vol. 6717, 67170, 2007.
32. Taminiau, T. H., F. D Stefani, and N. F. V. Hulst, "Single emitters coupled to plasmonic nano-antennas: Angular emission and collection efficiency," *New J. Phys.*, Vol. 10, 105005, 2008.
33. Huang, Y. and K. Boyle, "Popular antennas," *Antennas: From Theory to Practice*, 129–135, John Wiley & Sons Ltd, 2008.